

# Detection of Super-light Dark Matter Using Graphene Sensor

Doojin Kim,<sup>1,\*</sup> Jong-Chul Park,<sup>2,3,†</sup> Kin Chung Fong,<sup>4,5,‡</sup> and Gil-Ho Lee<sup>6,§</sup>

<sup>1</sup>*Mitchell Institute for Fundamental Physics and Astronomy,  
Department of Physics and Astronomy, Texas A&M University, College Station, TX 77843, USA*

<sup>2</sup>*Department of Physics and Institute of Quantum Systems,  
Chungnam National University, Daejeon 34134, Republic of Korea*

<sup>3</sup>*Particle Theory and Cosmology Group, Center for Theoretical Physics of the Universe,  
Institute for Basic Science (IBS), Daejeon, 34126, Republic of Korea*

<sup>4</sup>*Raytheon BBN Technologies, Quantum Information Processing Group, Cambridge, MA 02138, USA*

<sup>5</sup>*Department of Physics, Harvard University, Cambridge, MA 02138, USA*

<sup>6</sup>*Department of Physics, Pohang University of Science and Technology, Pohang 37673, Republic of Korea*

We propose a new dark-matter detection strategy that will enable the search of super-light dark matter  $m_\chi \simeq 0.1$  keV, representing an improvement of the minimum detectable mass by more than three order of magnitude over the ongoing experiments. This is possible by integrating intimately the target material,  $\pi$ -bond electrons in graphene, into a Josephson junction to achieve a high sensitivity detector that can resolve a small energy exchange from dark matter as low as  $\sim 0.1$  meV. We investigate detection prospects with pg-, ng- and  $\mu$ g-scale detectors by calculating the scattering rate between dark matter and free electrons confined in two-dimensional graphene with Pauli-blocking factors included. We find not only that the proposed detector can serve as a complementary probe of super-light dark matter but also achieve higher experimental sensitivities than other proposed experiments, thanks to the extremely low energy threshold of our Josephson junction sensor.

**Introduction.** While dark matter is a crucial ingredient of the universe and its cosmological history, the elusive nature of dark matter renders its detection via non-gravitational interactions rather challenging. A host of theoretical and experimental effort has been devoted to understanding the weakly interacting massive particles (WIMPs), mainly motivated by the so-called WIMP miracle. The null signal observations thus far set stringent bounds on dark-matter candidates of  $m_\chi \sim 10$  GeV – 100 TeV [1]. On the other hand, the dark-matter mass can range, in general, from  $10^{-22}$  eV to  $10^{68}$  eV [1], so the spotlight is directing gradually toward other mass scales.

Dark-matter candidates lying in the keV-to-MeV mass range have received particular attention. Most of the conventional dark-matter direct-detection experiments are nearly insensitive to the associated signal due to the energy threshold to overcome, and thus relevant dark-matter models are less constrained. Moreover, thermal production of such dark matter is still allowed. Many models containing dark-matter candidates of this mass scale have been proposed and addressing various interesting phenomenology; for example, self-/strongly-interacting dark matter [2, 3], dark-matter freeze-in production [4, 5], keV mirror-neutrino dark matter [6], MeV dark matter for the 511 keV  $\gamma$ -ray line [7], MeV secluded dark matter [8, 9], keV dark matter for the 3.5 keV X-ray line [10, 11], and elastically decoupling dark matter [12].

Direct searches of MeV-range light dark matter are being actively performed by e.g., DAMIC, DarkSide, EDELWEISS, SENSEI, SuperCDMS, and XENON1T Collaborations. However, experimental detection of keV-range “super-light” dark matter is very challenging as the expected energy deposition is of order meV – eV, requiring a tiny energy threshold. A handful of detection schemes have been proposed thus far [13–24], based on new technologies measuring small energy depositions in the detector. They assume that dark matter scatters off either electrons [13–19], nuclei [20–22] or phonons [23, 24] in the detector material. Various detector materials were investigated, including superconducting devices [13, 14, 19], superfluid helium [20–22], graphene [15, 18], carbon nanotube [16], three-dimensional Dirac materials [17] and polar materials [23, 24]. Although some of them may accommodate dark-matter events invoking meV-range energy depositions, the actual detection is essentially limited by the bolometer technology. The aforementioned proposals adopt sensors such as a transition-edge sensor (TES) [25], a microwave kinetic inductance device (MKID) [26], and a superconducting-nanowire single-photon detector (SNSPD) [27], with typical operation frequencies ranging from X-ray to near-infrared [28], from X-ray to far-infrared [29], and from ultraviolet to mid-infrared [30], respectively. To detect the energy deposition from dark matter as small as meV, i.e.  $\sim 240$  GHz, further R&D is therefore needed.

To extend the search of dark matter in lower mass regime, which has never been explored by dark-matter direct searches, we propose a new experimental strategy using a graphene-based Josephson-junction microwave single-photon detector [31]. It was recently demonstrated

\* doojin.kim@tamu.edu

† jcpark@cnu.ac.kr

‡ fongkc@gmail.com

§ lghman@postech.ac.kr

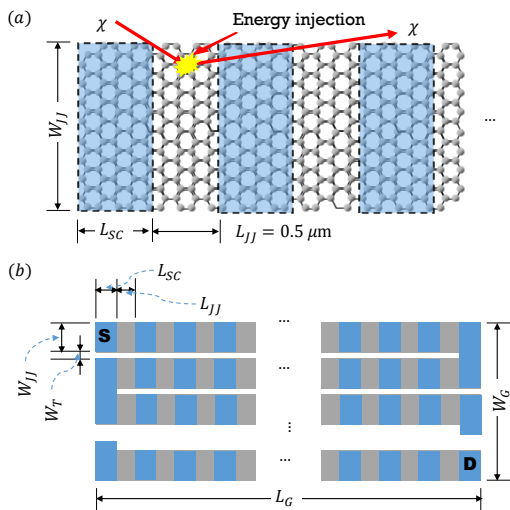


FIG. 1. (a) Schematic description of detection principle with a single strip. Dark matter scattering can induce an energy injection. (b) Schematic layout of a full detector unit.

in the laboratory that the GJJ device can have an energy resolution equivalent to sub-meV energy quanta [32]. Therefore, it is possible to design and embark on experiments aiming at detecting dark matter of  $m_\chi \gtrsim 0.1$  keV, using a sensor of higher Technology Readiness Level. We provide a conceptual detector-design proposal and study the detection prospects of super-light dark matter interacting with  $\pi$ -bond electrons not only at the proposed detector but at its smaller-version prototype.

**Detection principle.** A single unit of the device consists of a sheet of mono-layer graphene two sides of which are joined to superconducting material, forming a superconductor-normal metal-superconductor (SNS) Josephson junction (JJ) [31], as schematically shown in Figure 1(a). Basically, when injected energy raises the electron temperature in the graphene sheet, the calorimetric effect can switch the zero-voltage of JJ to resistive state with an appropriate level of bias current. Graphene is a mono-atomic layer of carbon atoms in a hexagonal structure [33, 34]. Its electronic band structure shows linear energy-momentum dispersion relationship which resembles to that of massless Dirac fermions in two-dimension. Near the Dirac point where the density of state vanishes, electronic heat capacity also vanishes. Due to the extremely suppressed electronic heat capacity of mono-layer graphene and its constricted thermal conductance to its phonons, the device is highly sensitive to small energy deposition. Very recently, Lee *et al.* [32] have demonstrated a microwave bolometer using GJJ with a noise equivalent power (NEP) corresponding to the thermodynamic limit. This NEP infers to the energy resolution of single 32-GHz (or equivalently,  $\sim 0.13$  meV) microwave photon in a single-photon detection mode.

If dark matter of interest couples to electrons, it can scatter off  $\pi$ -bond free electrons in the graphene sheet,

transferring some fraction of its incoming kinetic energy, i.e., the energy injection shown in Figure 1(a) takes place through dark matter scattering. The recoiling electron heats up and thermalizes with nearby electrons rapidly via electron-electron interactions within a few picoseconds [35, 36], and the JJ is triggered. The dark matter in the present universe floats around the earth with the typical velocity being  $\sim 10^{-3}c$ . Therefore, a dark-matter particle of order 1 keV carries a kinetic energy of order 1 meV [ $\approx 1 \text{ keV} \times (10^{-3})^2$ ] so that the GJJ device can possess the sensitivity to the signal induced even by sub-keV-range dark matter. To the best of our knowledge, no device ever known has exhibited the sensitivity of this level practically, so we expect that the microwave single-photon detector technology using GJJ enables us to explore parameter regions for super-light particle dark matter in the near future.

**Conceptual design proposal.** Inspired by the GJJ device, we propose a dark-matter detector which consists of a multitude of the GJJ devices. A single-detector unit is an assembly of a number of graphene strips of  $L_G \times W_{JJ}$  (fabricated from a graphene sheet of  $L_G \times W_G$  with trenches of  $W_T$ ) and superconducting-material strips of  $L_{SC} \times W_{JJ}$  with a pair of source “S” and drain “D” of the device, as shown in Figure 1(b). Superconducting strips of  $W_{JJ} = 3 \mu\text{m}$  ( $30 \mu\text{m}$ ) corresponding to a threshold energy of  $\sim 0.1$  meV (1 meV) are laid on a graphene strip by an interval of  $L_{JJ} = 0.5 \mu\text{m}$ , forming an array of superconducting-graphene-superconducting-graphene-superconducting- $\dots$  (SGSGS $\dots$ ). When the superconducting strip width increases, the area of graphene increases so the heat capacity also increases. Therefore, more energy is needed to trigger the GJJ device. Each sequence of SGS represents a single GJJ device. Note that all GJJs are connected in series so that even a single switched GJJ allows the series resistance measured between S and D to switch from 0 to a finite value. Technical details and fabrication feasibility are discussed in Supplemental. A larger-scale detector can be made of a stack of such detector units.

Our sensitivity study is aiming at ng-scale and  $\mu\text{g}$ -scale detectors, while a pg-scale prototype detector will be prepared first to test the feasibility of building a multi-device detector. To prepare for the unit forming a  $\mu\text{g}$ -scale graphene device, one needs a total of  $\sim 6 \text{ cm} \times 6 \text{ cm}$  sheet of graphene. This can be grown by commercial technology, e.g., chemical vapor depositions [37, 38]. We, therefore, expect that  $\mu\text{g}$ -scale detectors will be constructible in the near future.

Since the GJJ bolometer is extremely sensitive to small changes in temperature, it is crucial to keep the system temperature low enough to suppress potential thermal backgrounds or noise. To this end, we place the detector in the cryogenic surroundings by cooling the detector system down to  $\sim 10$  mK using dilution refrigerators. Further, external electromagnetic noise can be sufficiently suppressed by RF electrical filtering, mu-

metal shielding, etc which have been well developed for quantum computing and information technologies. An irreducible background may arise from the solar neutrinos (mostly  $pp$  neutrinos) scattering off an electron and depositing a small amount of energy [39]. However, considering the volume of the detector at hand, the expected number of background events is negligible ( $\lesssim \mathcal{O}(10^{-7}) \mu\text{g}^{-1}\text{year}^{-1}$ ) [14, 40].

We remark that in our study here the proposed detector plays a role of not only the bolometer to measure the temperature change or the single-photon detector to count the number of scattering events, but target material off which dark matter scatters. Alternatively, this can be used only for a bolometer or a single-photon detector in other dark-matter detection proposals by coupling it to the target material such as superconductors, superfluid helium, or polar materials in Refs. [14], [20], and [23], respectively. In this case, energetic quasiparticles generated in the target material by dark matter get absorbed into graphene, followed by increasing the electronic temperature of the graphene and triggering GJJ.

**Experimental sensitivities.** Our interest here is the event counts via the interaction between dark matter and  $\pi$ -bond electrons in the graphene which can behave like free electrons. Dark matter may deposit energy via scattering off the  $\sigma$ -bond electrons, making an additional contribution to the signal sensitivity. However, we conservatively restrict our analysis to the former channel to demonstrate the usefulness of the GJJ-based detector as a super-light dark-matter detector, while deferring a full analysis for a future publication.

While our calculations basically follow the procedure formulated in Refs. [13, 14], we modify them wherever the two-dimensional nature of graphene is relevant. The total expected event count per unit mass per unit time,  $n_{\text{eve}}$  is given by

$$n_{\text{eve}} = \int dE_r dv_{\chi\parallel} \frac{d\langle n_{\text{gr}}^e \sigma v_{\text{rel}\parallel} \rangle}{dE_r} \frac{1}{a_{\text{gr}}} \frac{\rho_{\chi}}{m_{\chi}} f_{\text{MB}}(v_{\chi\parallel}), \quad (1)$$

where  $n_{\text{gr}}^e$  is the number density of target electrons per unit area and  $a_{\text{gr}} = 7.62 \times 10^{-8} \text{ g}\cdot\text{cm}^{-2}$  is the areal density of graphene.  $m_{\chi}$  is the mass of dark matter and  $\rho_{\chi}$  is the local dark-matter energy density which is chosen to be  $0.3 \text{ GeV}\cdot\text{cm}^{-3}$  throughout our analysis.  $f_{\text{MB}}(v_{\chi\parallel})$  is the graphene-surface-parallel velocity profile of dark matter for which we take a plane-projection of a modified Maxwell-Boltzmann distribution  $F_{\text{MB}}$  [41] with root-mean-square velocity  $v_0 = 220 \text{ km}\cdot\text{s}^{-1}$  and escape velocity  $v_{\text{esc}} = 550 \text{ km}\cdot\text{s}^{-1}$  (see Supplemental):

$$f_{\text{MB}}(v_{\chi\parallel}) = \int_{-\sqrt{1-(v_{\chi\parallel}/v_{\text{esc}})^2}}^{\sqrt{1-(v_{\chi\parallel}/v_{\text{esc}})^2}} d \cos \theta \frac{1}{2 \sin \theta} F_{\text{MB}} \left( \frac{v_{\chi\parallel}}{\sin \theta} \right), \quad (2)$$

where  $\theta$  is the angle between the incoming dark-matter direction and the graphene-surface-normal direction. Finally, the velocity-averaged event rate on a (sufficiently

thin) graphene sheet per unit time  $\langle n_{\text{gr}}^e \sigma v_{\text{rel}\parallel} \rangle$  is

$$\langle n_{\text{gr}}^e \sigma v_{\text{rel}\parallel} \rangle = \int \frac{d^3 p_{\chi,f}}{(2\pi)^3} \frac{|\overline{\mathcal{M}}|^2}{16m_e^2 m_{\chi}^2} S_{\text{gr}}(E_r, q), \quad (3)$$

where  $p_{\chi,f}$  is the momentum of final-state dark matter and where all the total energy quantities are taken in the non-relativistic limit. Here  $|\overline{\mathcal{M}}|^2$  denotes the matrix element for the scattering process between dark matter and free electrons. The Pauli-blocking effects are encoded in  $S_{\text{gr}}(E_r, q)$ , a structure function over electron-recoil kinetic energy  $E_r$  and the magnitude of momentum transfer along the graphene surface  $q = |\vec{p}_{\chi\parallel,i} - \vec{p}_{\chi\parallel,f}|$  with a subscript  $i$  implying the initial state. It is then convenient to convert  $d^3 p_{\chi,f}$  to  $dE_r$  and  $dq$ :

$$\frac{d^3 p_{\chi,f}}{(2\pi)^3} \rightarrow \frac{dE_r dq}{(2\pi)^2} \frac{2q(E_{\chi,i} - E_r)}{\tilde{\lambda}(q^2, p_{\chi,i}^2, p_{\chi,f}^2)}, \quad (4)$$

where  $\tilde{\lambda}(x, y, z) = \sqrt{2(xy + yz + zx) - x^2 - y^2 - z^2}$  and where we integrate out  $p_{\chi,f}^z$  by pulling out the delta-function factor in  $S_{\text{gr}} = (2\pi)\delta(p_{\chi,i}^z - p_{\chi,f}^z) \cdot S$  (see Supplemental). We next take the analytic expression for  $S$  derived in Ref. [14] based on Ref. [42]:

$$S(E_r, q) = \frac{m_e^2 T}{\pi q} \left[ \frac{E_r/T}{1 - \exp(-E_r/T)} \left( 1 + \frac{\xi}{E_r/T} \right) \right], \quad (5)$$

where  $T$  is the system temperature surrounding the detector which we take to be 10 mK as mentioned earlier. The  $\xi$  quantity is given by

$$\xi = \log \left[ \frac{1 + e^{(\epsilon_- - \mu)/T}}{1 + e^{(\epsilon_- + E_r - \mu)/T}} \right] \quad (6)$$

with

$$\epsilon_- = \frac{1}{4} \frac{\{E_r - q^2/(2m_e)\}^2}{q^2/(2m_e)}. \quad (7)$$

Here  $\mu$  is the chemical potential which is identified as the Fermi energy  $E_F$  at zero temperature. For a two-dimensional object like graphene, the linear energy-momentum dispersion suggests  $E_F = v_F \sqrt{\pi n_c}$ . Here the Fermi velocity of graphene  $v_F$  is  $1.15 \times 10^8 \text{ cm}\cdot\text{s}^{-1}$  [43] and carrier density  $n_c$  is chosen to be  $10^{12} \text{ cm}^{-2}$  [32].

We are now in the position to study dark-matter signal sensitivities which would be achieved by the proposed GJJ detector. We assume that dark matter interacts with electrons via an exchange of mediator  $\phi$  whose mass is  $m_{\phi}$ , as in many of the preceding studies. In the non-relativistic limit, the scattering cross section between free electrons and say, fermionic dark matter  $\chi$  is given by

$$\sigma_{e\chi} \approx \frac{g_e^2 g_{\chi}^2}{\pi} \frac{\mu_{e\chi}^2}{(m_{\phi}^2 + q^2)^2}, \quad (8)$$

where  $g_e$  and  $g_{\chi}$  parameterize couplings of  $\phi$  to electrons and  $\chi$  and where  $\mu_{e\chi}$  is the reduced mass of the electron- $\chi$  system. If the mediator is heavy enough such that

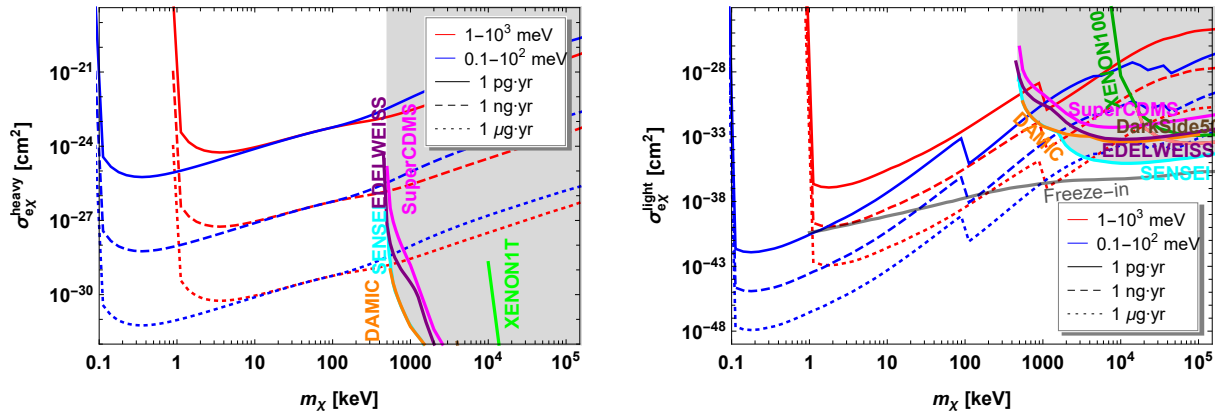


FIG. 2. Sensitivities of the proposed GJJ detector to 0.1 keV – 0.1 GeV dark matter in the plane of dark-matter mass  $m_\chi$  and scattering cross section between dark matter and electrons  $\sigma_{e\chi}$ . The dark matter is assumed to scatter off  $\pi$ -bond electrons in graphene, which can behave like free electrons, via an exchange of a heavy mediator (left panel) or a light mediator (right panel). Blue (red) curves show the sensitivities with electron kinetic energy deposition falling in 0.1 meV – 0.1 eV (1 meV – 1 eV), and solid, dashed, and dotted curves are for 1 pg, 1 ng, and 1  $\mu$ g GJJ detectors, respectively, with a year exposure. For comparison, we show the relic abundance line explained by freeze-in [40] and the existing limits [44] (gray region) from DAMIC, DarkSide50, EDLWEISS, SENSEI, SuperCDMS, XENON100, and XENON1T.

$m_\phi^2 \gg q^2$ , Eq. (8) is simplified to

$$\sigma_{e\chi}^{\text{heavy}} \approx \frac{g_e^2 g_\chi^2 \mu_{e\chi}^2}{\pi m_\phi^4}. \quad (9)$$

On the other hand, for the opposite limit or the light-mediator case (i.e.,  $m_\phi^2 \ll q^2$ ), we get

$$\sigma_{e\chi}^{\text{light}} \approx \frac{g_e^2 g_\chi^2 \mu_{e\chi}^2}{\pi q^4}. \quad (10)$$

The matrix element in Eq. (3) is related to the scattering cross section in Eq. (8) as

$$\sigma_{e\chi} = \frac{1}{16\pi} \frac{|\overline{\mathcal{M}}|^2}{m_e^2 m_\chi^2} \mu_{e\chi}^2. \quad (11)$$

To estimate our sensitivity reach, we take Eqs. (9) and (10) as the reference cross sections. For the light-mediator case, we replace the  $q$ -dependence by a reference value  $q_{\text{ref}} = \alpha_e m_e$  with  $\alpha_e$  being the usual electromagnetic fine-structure constant, following the prescription in Refs. [19, 40].

Figure 2 displays the sensitivities of the proposed GJJ detector to 0.1 keV – 0.1 GeV dark matter in the plane of dark-matter mass  $m_\chi$  and scattering cross section  $\sigma_{e\chi}$ . For estimating sensitivity reaches, we require 3.6 signal events which correspond to the 95% C.L. upper limit under the assumption of a null event observation over negligible neutrino-induced background events with Poisson statistics [45]. As mentioned before, such dark matter is assumed to interact with the  $\pi$ -bond electrons in the graphene target through an exchange of  $\phi$ . The left and the right panels are for the heavy- and the light-mediator cases, respectively. In both panels, the blue (red) curves

show the sensitivities with electron kinetic-energy deposition being in-between 0.1 meV and 0.1 eV (1 meV and 1 eV), i.e., the superconducting strips of the GJJ detector have  $\ell = 3 \mu\text{m}$  ( $\ell = 30 \mu\text{m}$ ). The solid, dashed, and dotted curves are the expected results with 1 pg-scale, 1 ng-scale, and 1  $\mu$ g-scale detectors exposed for a year, respectively. For reference purposes, we exhibit the relic abundance line explained by freeze-in [40] and the existing bounds [44] together from DAMIC, DarkSide50, EDLWEISS, SENSEI, SuperCDMS, XENON100, and XENON1T by the orange, brown, purple, cyan, pink, dark green, and green lines, respectively.

**Discussion.** We remark that cosmological and astrophysical observations provide bounds on super-light dark matter while the aforementioned dark-matter direct-search experiments are exploring  $m_\chi - \sigma_{e\chi}$  space. For example, the so-called Lyman- $\alpha$  forest is a powerful tool to constrain keV-range dark matter which was thermally produced in the early universe. Such “warm” dark matter appears relativistic when freezes out, so it may affect the structure formation, leaving appreciable differences in the Lyman- $\alpha$  absorption features from what is observed today (see, e.g., Ref. [46]). Currently, warm dark matter of  $m_\chi \lesssim \mathcal{O}(\text{keV})$  is disfavored by Lyman- $\alpha$  forests, while there still exist relatively large uncertainties even among very recent results: e.g., Ref. [47] claims that  $m_\chi > 10 \text{ keV}$  is allowed at 95% C.L., whereas Ref. [48] claims  $m_\chi > 1.9 \text{ keV}$  is allowed at 95% C.L.. In fact, the proposed GJJ detector enables to probe 1 – 10 keV dark matter very efficiently by lowering the threshold to 0.1 meV, as compared to dark-matter detectors adopting other bolometer technologies. This is because a lower threshold allows to access the phase space associated with recoil electrons carrying smaller energy. This is also

clearly demonstrated by the red (higher threshold) and the blue (lower threshold) curves in Figure 2.

By contrast, if dark matter is produced non-thermally, the bounds from the Lyman- $\alpha$  forest are generically irrelevant. It is therefore important to explore the  $\mathcal{O}(\text{keV})$  mass region in a model-independent sense. There are many well-motivated physics models containing such non-thermal super-light dark-matter candidates (see Ref. [49] for a recent review): for example, sterile neutrinos, super-light dark gauge bosons, axion-like dark-matter particles, and axino/gravitino dark matter. We expect that search strategies using the proposed GJJ detector can provide a probe complementary to the existing experimental effort for such dark-matter candidates.

We emphasize an implication of our simplified model of scattering between dark matter moving in 3-dimensional space and free electrons confined in the 2-dimensional graphene sheet. As stated earlier, the momentum transfer  $q$  in Eq. (3) is mainly determined by the change of the  $\chi$ -momentum component parallel to the graphene surface. Therefore, the device sensitivity to the dark-matter signal will be maximized (minimized) when  $\chi$  is incident in the direction parallel (perpendicular) to the graphene surface. In other words, the dark-matter signal would be validated by (actively) rotating such that the graphene sheet is aligned with the direction parallel or perpendicular to the overall dark-matter flux and checking the directional dependence of event rates. We reserve further investigations on this interesting possibility and detailed subleading effects beyond our simplified scattering model for a future publication.

Finally, we point out that the proposed detector is capable of detecting even lighter dark matter candidates of sub-meV – eV mass. For example, axion-like particle or dark gauge boson dark matter candidates within such a mass range can be absorbed to the detector material via a Compton-like process with an electron resulting in an emission of a photon, i.e.,  $\chi + e \rightarrow \gamma + e$ . Here the radiated photon is typically as energetic as the mass energy of the incoming dark matter, so the proposed detector may have decent sensitivities to these dark matter candidates. Note that if the mass of the absorbed dark matter particle is greater than the binding energy of an electron, i.e.,  $\mathcal{O}(\text{eV})$ , an electron is ejected via a process analogous to the photoelectric effect [50–53]. Numerous dark matter direct detection experiments have conducted searches for such ejected electron signals, and our proposal can offer a new avenue for this search effort.

**Conclusions.** In conclusion, we have proposed a class of *new* dark matter detectors, adopting the GJJ device which has been implemented and demonstrated experimentally. Due to its outstanding sensitivity to energy changes as small as  $\sim 0.1$  meV, the proposed detectors made of an array of GJJ devices are, for the first time, capable of probing dark matter candidates as light as  $\sim 0.1$  keV via the scattering of dark matter off electrons. We have shown that the sensitivity of detec-

tors of 1- $\mu\text{g}$  graphene can reach  $\sigma_{e\chi} \approx 10^{-31}$   $\text{cm}^{-2}$  and  $\sigma_{e\chi} \approx 10^{-48}$   $\text{cm}^{-2}$  for the heavy and the light mediator cases, with one-year exposure. In particular, even the 1 pg-scale detector can probe the prediction of freeze-in scenarios for the light mediator case. As a final remark, we are now developing a prototypical detector of bigger SNS JJ multiplicity, along with more dedicated background studies and extended investigations of various dark-matter candidates which can be detected by the proposed detectors.

**Acknowledgments.** We would like to thank Kaushtubh Agashe, Bhaskar Dutta and Yue Zhao for their careful reading of the draft and insightful discussions. We also would like to thank Rupak Mahapatra and Yonit Hochberg for their useful comments and discussions. This work was performed in part at the Aspen Center for Physics, which is supported by National Science Foundation grant PHY-1607611. Part of this work was discussed in the workshop “Dark Matter as a Portal to New Physics” at the Asia Pacific Center for Theoretical Physics. The work of DK is supported by the U.S. Department of Energy Grant DE-SC0010813. JCP and GHL acknowledges the support from Samsung Science and Technology Foundation (Project No. SSTF-BA2101-06). The work is supported by the National Research Foundation of Korea (NRF) [NRF-2019R1C1C1005073 (JCP), NRF-2020M3H3A1100839 (GHL)]. KCF acknowledges the support from the Army Research Office under Cooperative Agreement Number W911NF-17-1-0574.

## SUPPLEMENTAL MATERIAL

**Detector design details.** We provide more technical details for building a large-scale detector consisting of numerous GJJ units. We show a possible architecture for making  $\sim 10^9$  GJJs, the number that would be required for a  $\mu\text{g}$ -scale detector. As shown in Figure 3, we begin with a wafer-scale graphene<sup>1</sup> grown on an 4-inch silicon wafer covered with  $\text{SiO}_2$  insulating layers, and assume that graphene is in square shape, width  $W_G = 6$  cm by length  $L_G = 6$  cm, for simplicity of our calculation. Narrow trenches of width  $W_T = 0.5$   $\mu\text{m}$  can be cut to make multiple strips of graphene of width  $W_{JJ} = 3$   $\mu\text{m}$ . The superconducting electrode can be deposited in such a way that all the GJJs are connected in series using the superconducting electrode of length  $L_{SC} = 0.5$   $\mu\text{m}$  and GJJ length  $L_{JJ} = 0.5$   $\mu\text{m}$ . As the smallest feature would be 500 nm, either electron beam lithography (for example, the ELS-F150 model from Elionix can make 4 nm features and support an 8 inch wafer) or photo-lithography

<sup>1</sup> Chemical vapor deposition grown single layer graphene of 1 m  $\times$  1 m is already available in the market such as Graphene Square [54].

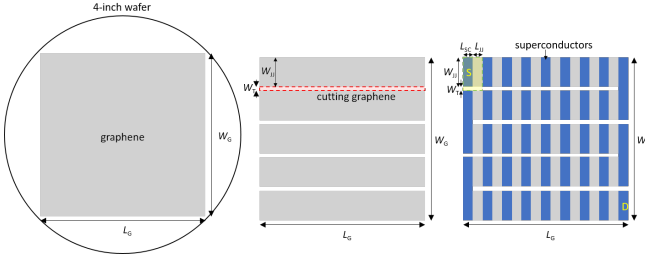


FIG. 3. Schematics of possible fabrication procedure. Schematics are not in scale. (a) A graphene sheet of  $W_G \times L_G$  grown on 4-inch wafer. (b) The etched graphene represented by a box outlined by dotted red line. (c) A superconductor-loaded full detector unit.

(50 nm features can be made with deep ultraviolet light) can be used.

As also mentioned in the main manuscript, it is important to note that all the GJJs are connected in series not in parallel such that even with only one GJJ switched on, the series resistance measured between source ‘‘S’’ and drain ‘‘D’’ will switch from zero to a finite value. More specifically, we bias a DC current and monitor the DC voltage between the S electrode (i.e., the very first superconducting electrode) and the D electrode (i.e., the very last superconducting electrode). Due to the self-heating of GJJ in a resistive state, GJJ will stay in resistive state after it switches from a supercurrent state to a resistive state. If any one of GJJs switches, DC voltage will spike up to some finite value since all the GJJs are connected in series, and this voltage can be easily detected even with a slow DC measurement.

The total number of GJJs on a single wafer  $N_W$  is

$$N_W = \frac{W_G L_G}{(W_T + W_{JJ})(L_{SC} + L_{JJ})} \approx 1.03 \times 10^9, \quad (12)$$

which is comparable to or less than the number of transistors in modern integrated circuit chips ( $\sim 5-10 \times 10^9$ ) and the structure of GJJ is much simpler than the transistors with gates. We therefore expect that the currently available nano-fabrication technology can achieve the device that we propose. One example device consisting of multiple Josephson junctions is the voltage standard: about 20,000 Josephson junctions were fabricated for realizing a 12 V voltage standard [55].

Large enough dilution refrigerator to cool down the whole device down to 10 mK temperature is already available in the market. For example, the Proteox model from Oxford Instruments has a mixing chamber plate of diameter of 360 mm, the XLD model from Bluefors has a mixing chamber plate of diameter of 500 mm, and the CF-CS110 model from Leiden Cryogenics has a mixing chamber plate of diameter of 490 mm.

**Projected Maxwell-Boltzmann distribution.** When a dark matter particle of velocity  $v_\chi$  is incident on a graphene sheet by angle  $\theta$  with respect to the plane-normal direction, the parallel component, i.e.,  $v_{\chi\parallel} =$

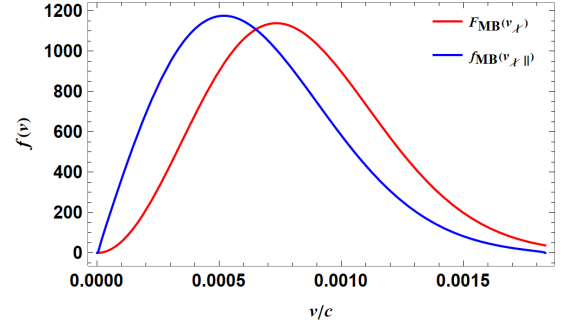


FIG. 4. Comparison between  $F_{MB}(v_\chi)$  and  $f_{MB}(v_{\chi\parallel})$ .

$v_\chi \sin \theta$ , is involved in the momentum transfer. Denoting the probability density in  $v_{\chi\parallel}$  by  $f_{MB}(v_{\chi\parallel}) = \frac{dP}{dv_{\chi\parallel}}$ , we find that

$$\frac{dP}{dv_{\chi\parallel}} = \int \frac{dv_\chi}{dv_{\chi\parallel}} \frac{d^2 P}{dv_\chi d\Omega} d\Omega = \int \frac{1}{\sin \theta} \frac{d^2 P}{dv_\chi d\Omega} d\Omega, \quad (13)$$

where  $\frac{dP}{dv_\chi}$  is a modified Maxwell-Boltzmann distribution  $F_{MB}$  [41] and  $\frac{d^2 P}{dv_\chi d\Omega}$  is the distribution per unit solid angle:

$$\frac{F_{MB}(v_\chi)}{4\pi} = \frac{v_\chi^2 \exp\left(-\frac{v_\chi^2}{v_0^2}\right)}{\pi^{3/2} v_0^3 \left[ \operatorname{erf}\left(\frac{v_{esc}}{v_0}\right) - \frac{2}{\sqrt{\pi}} \frac{v_{esc}}{v_0} \exp\left(-\frac{v_{esc}^2}{v_0^2}\right) \right]}, \quad (14)$$

To evaluate  $f_{MB}$  at  $v_{\chi\parallel}$ , we have to integrate over all relevant  $\theta$  and azimuth  $\varphi$  values:

$$f_{MB}(v_{\chi\parallel}) = \int_0^{2\pi} d\varphi \int_{\cos \theta_-}^{\cos \theta_+} d \cos \theta \frac{1}{\sin \theta} \frac{F_{MB}\left(\frac{v_\chi}{\sin \theta}\right)}{4\pi}, \quad (15)$$

where  $\cos \theta_\pm = \pm \sqrt{1 - \left(\frac{v_{\chi\parallel}}{v_{esc}}\right)^2}$ .

We show a comparison between our projected distribution  $f_{MB}(v_{\chi\parallel})$  (blue curve) and the original distribution  $F_{MB}(v_\chi)$  (red curve) in Figure 4. As expected, the graphene plane-parallel component  $v_{\chi\parallel}$  populates more in the lower velocity region.

**Structure function.** The structure-function for the graphene system of interest  $S_{gr}$  is given by

$$S_{gr}(E_r, q) = 2 \int \frac{d^3 p_{e,i}}{(2\pi)^3} \int \frac{d^3 p_{e,f}}{(2\pi)^3} (2\pi) \delta(p_{e,i}^z - p_{e,f}^z) \\ \times (2\pi)^4 \delta^{(4)}(p_{\chi,i} + p_{e,i} - p_{\chi,f} - p_{e,f}) \\ \times f_{e,i}(E_{e,i}) \{1 - f_{e,f}(E_{e,f})\}, \quad (16)$$

where  $p_{e,i(f)}$  denotes the momentum of the initial-state (final-state) electron. The delta function in the first line reflects the assumption that the free electrons are confined in the graphene surface, or equivalently, they do not get any significant momentum change along the

surface-normal direction, as far as the electron recoil kinetic energy is sufficiently smaller than the work function of graphene. The Fermi-Dirac distribution functions for the initial-state (final-state) electrons  $f_{e,i(f)}$  are

$$f_{e,i(f)} = \left\{ 1 + \exp \left( \frac{E_{e,i(f)} - \mu}{T} \right) \right\}^{-1}, \quad (17)$$

where  $\mu$  and  $T$  are the chemical potential and the system temperature, respectively. Integrating over  $d^3p_{e,f}$  in combination with the spatial components of the four-dimensional delta function yields

$$\begin{aligned} S_{\text{gr}}(E_r, q) &= (2\pi)\delta(p_{\chi,i}^z - p_{\chi,f}^z) \cdot \frac{1}{2\pi^2} \int d^3p_{e,i} \\ &\times \delta(E_r + E_{\chi,i} - E_{\chi,f}) f_{e,i}(E_{e,i}) \{1 - f_{e,f}(E_{e,f})\} \\ &\equiv (2\pi)\delta(p_{\chi,i}^z - p_{\chi,f}^z) \cdot S(E_r, q), \end{aligned} \quad (18)$$

where we factor out the delta function of  $p_{\chi,f}^z$ , which is used for the  $d^3p_{\chi,f}$  integral, and separately define  $S(E_r, q)$ . The closed form for  $S(E_r, q)$  is available in the non-relativistic limit [42], as shown in Eq. (6) of the main article.

- 
- [1] M. Battaglieri et al. (2017) arXiv:1707.04591 [hep-ph].
- [2] E. D. Carlson, M. E. Machacek, and L. J. Hall, *Astrophys. J.* **398**, 43 (1992).
- [3] Y. Hochberg, E. Kufflik, T. Volansky, and J. G. Wacker, *Phys. Rev. Lett.* **113**, 171301 (2014), arXiv:1402.5143 [hep-ph].
- [4] T. Moroi, H. Murayama, and M. Yamaguchi, *Phys. Lett.* **B303**, 289 (1993).
- [5] L. J. Hall, K. Jedamzik, J. March-Russell, and S. M. West, *JHEP* **03**, 080 (2010), arXiv:0911.1120 [hep-ph].
- [6] Z. G. Berezhiani and R. N. Mohapatra, *Phys. Rev.* **D52**, 6607 (1995), [,279(1995)], arXiv:hep-ph/9505385 [hep-ph].
- [7] C. Boehm, D. Hooper, J. Silk, M. Casse, and J. Paul, *Phys. Rev. Lett.* **92**, 101301 (2004), arXiv:astro-ph/0309686 [astro-ph].
- [8] J.-H. Huh, J. E. Kim, J.-C. Park, and S. C. Park, *Phys. Rev.* **D77**, 123503 (2008), arXiv:0711.3528 [astro-ph].
- [9] M. Pospelov, A. Ritz, and M. B. Voloshin, *Phys. Lett.* **B662**, 53 (2008), arXiv:0711.4866 [hep-ph].
- [10] J.-C. Park, S. C. Park, and K. Kong, *Phys. Lett.* **B733**, 217 (2014), arXiv:1403.1536 [hep-ph].
- [11] D. Kim and J.-C. Park, *Phys. Lett.* **B750**, 552 (2015), arXiv:1508.06640 [hep-ph].
- [12] E. Kufflik, M. Perelstein, N. R.-L. Lorier, and Y.-D. Tsai, *Phys. Rev. Lett.* **116**, 221302 (2016), arXiv:1512.04545 [hep-ph].
- [13] Y. Hochberg, Y. Zhao, and K. M. Zurek, *Phys. Rev. Lett.* **116**, 011301 (2016), arXiv:1504.07237 [hep-ph].
- [14] Y. Hochberg, M. Pyle, Y. Zhao, and K. M. Zurek, *JHEP* **08**, 057 (2016), arXiv:1512.04533 [hep-ph].
- [15] Y. Hochberg, Y. Kahn, M. Lisanti, C. G. Tully, and K. M. Zurek, *Phys. Lett.* **B772**, 239 (2017), arXiv:1606.08849 [hep-ph].
- [16] G. Cavoto, F. Luchetta, and A. D. Polosa, *Phys. Lett.* **B776**, 338 (2018), arXiv:1706.02487 [hep-ph].
- [17] Y. Hochberg, Y. Kahn, M. Lisanti, K. M. Zurek, A. G. Grushin, R. Ilan, S. M. Griffin, Z.-F. Liu, S. F. Weber, and J. B. Neaton, *Phys. Rev.* **D97**, 015004 (2018), arXiv:1708.08929 [hep-ph].
- [18] E. Baracchini et al. (PTOLEMY), (2018), arXiv:1808.01892 [physics.ins-det].
- [19] Y. Hochberg, I. Charaev, S.-W. Nam, V. Verma, M. Colangelo, and K. K. Berggren, (2019), arXiv:1903.05101 [hep-ph].
- [20] K. Schutz and K. M. Zurek, *Phys. Rev. Lett.* **117**, 121302 (2016), arXiv:1604.08206 [hep-ph].
- [21] S. Knapen, T. Lin, and K. M. Zurek, *Phys. Rev.* **D95**, 056019 (2017), arXiv:1611.06228 [hep-ph].
- [22] H. J. Maris, G. M. Seidel, and D. Stein, *Phys. Rev. Lett.* **119**, 181303 (2017), arXiv:1706.00117 [astro-ph.IM].
- [23] S. Knapen, T. Lin, M. Pyle, and K. M. Zurek, *Phys. Lett.* **B785**, 386 (2018), arXiv:1712.06598 [hep-ph].
- [24] S. Griffin, S. Knapen, T. Lin, and K. M. Zurek, *Phys. Rev.* **D98**, 115034 (2018), arXiv:1807.10291 [hep-ph].
- [25] D. H. Andrews, W. F. Brucksch, W. T. Ziegler, and E. R. Blanchard, *Review of Scientific Instruments* **13**, 281 (1942).
- [26] P. K. Day, H. G. LeDuc, B. A. Mazin, A. Vayonakis, and J. Zmuidzinas, *Nature* **425**, 817 (2003).
- [27] G. N. Gol'tsman, O. Okunev, G. Chulkova, A. Lipatov, A. Semenov, K. Smirnov, B. Voronov, A. Dzardanov, C. Williams, and R. Sobolewski, *Applied Physics Letters* **79**, 705 (2001).
- [28] T. Gerrits, A. Lita, B. Calkins, and S. W. Nam, "Superconducting transition edge sensors for quantum optics," in *Superconducting Devices in Quantum Optics*, edited by R. H. Hadfield and G. Johansson (Springer International Publishing, 2016) pp. 31–60.
- [29] J. Zmuidzinas, *Annual Review of Condensed Matter Physics* **3**, 169 (2012).
- [30] I. Holzman and Y. Ivry, *Technol.* **2019**, 1800058 (2018), arXiv:1807.09060 [physics.ins-det].
- [31] E. D. Walsh, D. K. Efetov, G.-H. Lee, M. Heuck, J. Crossno, T. A. Ohki, P. Kim, D. Englund, and K. C. Fong, *Phys. Rev. Applied* **8**, 024022 (2017).
- [32] G.-H. Lee, D. K. Efetov, W. Jung, L. Ranzani, E. D. Walsh, T. A. Ohki, T. Taniguchi, K. Watanabe, P. Kim, D. Englund, and K. C. Fong, *Nature* **586**, 42 (2020), arXiv:1909.05413 [cond-mat].

- [33] K. S. Novoselov, A. K. Geim, S. V. Morozov, D. Jiang, M. I. Katsnelson, I. V. Grigorieva, S. V. Dubonos, and A. A. Firsov, *Nature* **438**, 197 (2005), arXiv:cond-mat/0509330 [cond-mat.mes-hall].
- [34] Y. Zhang, Y.-W. Tan, H. L. Stormer, and P. Kim, *Nature* **438**, 201 (2005), arXiv:cond-mat/0509355 [cond-mat.mes-hall].
- [35] K. J. Tielrooij, J. C. W. Song, S. A. Jensen, A. Centeno, A. Pesquera, A. Zurutuza Elorza, M. Bonn, L. S. Levitov, and F. H. L. Koppens, *Nature Physics* **9**, 248 (2013).
- [36] D. Brida et al., *Nature Communications* **4**, 1987 (2013).
- [37] K. S. Kim, Y. Zhao, H. Jang, S. Y. Lee, J. M. Kim, K. S. Kim, J.-H. Ahn, P. Kim, J.-Y. Choi, and B. H. Hong, *Nature* **457**, 706 (2009).
- [38] S. Bae et al., *Nature Nanotechnology* **5**, 574 (2010).
- [39] J. N. Bahcall, *Phys. Rev.* **C56**, 3391 (1997), arXiv:hep-ph/9710491 [hep-ph].
- [40] R. Essig, J. Mardon, and T. Volansky, *Phys. Rev.* **D85**, 076007 (2012), arXiv:1108.5383 [hep-ph].
- [41] M. C. Smith et al., *Mon. Not. Roy. Astron. Soc.* **379**, 755 (2007), arXiv:astro-ph/0611671 [astro-ph].
- [42] S. Reddy, M. Prakash, and J. M. Lattimer, *Phys. Rev.* **D58**, 013009 (1998), arXiv:astro-ph/9710115 [astro-ph].
- [43] S. Kim, I. Jo, D. C. Dillen, D. A. Ferrer, B. Fallahazad, Z. Yao, S. K. Banerjee, and E. Tutuc, *Phys. Rev. Lett.* **108**, 116404 (2012).
- [44] Dark Matter Limit Plotter, <https://supercdms.slac.stanford.edu/dark-matter-limit-plotter>.
- [45] G. J. Feldman and R. D. Cousins, *Phys. Rev.* **D57**, 3873 (1998), arXiv:physics/9711021 [physics.data-an].
- [46] A. Boyarsky, J. Lesgourgues, O. Ruchayskiy, and M. Viel, *JCAP* **0905**, 012 (2009), arXiv:0812.0010 [astro-ph].
- [47] N. Palanque-Desabrouille, C. Yèche, N. Schöneberg, J. Lesgourgues, M. Walther, S. Chabanier, and E. Armengaud, (2019), arXiv:1911.09073 [astro-ph.CO].
- [48] A. Garzilli, O. Ruchayskiy, A. Magalich, and A. Boyarsky, (2019), arXiv:1912.09397 [astro-ph.CO].
- [49] H. Baer, K.-Y. Choi, J. E. Kim, and L. Roszkowski, *Phys. Rept.* **555**, 1 (2015), arXiv:1407.0017 [hep-ph].
- [50] S. Dimopoulos, G. D. Starkman, and B. W. Lynn, *Phys. Lett.* **168B**, 145 (1986).
- [51] F. T. Avignone, III, R. L. Brodzinski, S. Dimopoulos, G. D. Starkman, A. K. Drukier, D. N. Spergel, G. Gelmini, and B. W. Lynn, *Phys. Rev.* **D35**, 2752 (1987).
- [52] M. Pospelov, A. Ritz, and M. B. Voloshin, *Phys. Rev.* **D78**, 115012 (2008), arXiv:0807.3279 [hep-ph].
- [53] I. M. Bloch, R. Essig, K. Tobioka, T. Volansky, and T.-T. Yu, *JHEP* **06**, 087 (2017), arXiv:1608.02123 [hep-ph].
- [54] Graphene Square, <http://www.graphenesq.com>.
- [55] C. A. Hamilton, F. L. Lloyd, K. Chieh, and W. C. Goeke, *IEEE Transactions on Instrumentation and Measurement* **38**, 314 (1989).